Emission of terahertz-frequency electromagnetic radiation from bulk $Ga_xIn_{1-x}As$ crystals

Youngok Ko,[1] Suranjana Sengupta,[2] Stephanie Tomasulo,[2] Partha Dutta,[1] and Ingrid Wilke[2]
[1]*Electrical, Computer and System Engineering Department, Rensselaer Polytechnic Institute, 110 8th Street, Troy, New York 12180, USA*
[2]*Department of Physics, Applied Physics and Astronomy, Rensselaer Polytechnic Institute, 110 8th Street, Troy, New York 12180, USA*

(Received 29 April 2008; published 1 July 2008)

We report an experimental study of femtosecond optically excited emission of terahertz frequency electromagnetic radiation from $Ga_xIn_{1-x}As$ bulk crystals with alloy composition in the range between $0<x<0.65$. The terahertz-emission mechanisms in bulk $Ga_xIn_{1-x}As$ were studied as a function of carrier mobility, carrier concentrations, band gap as well as polycrystal grain size. Our experiments and analysis demonstrate that optical rectification is the dominant terahertz-emission mechanism for $Ga_xIn_{1-x}As$ with $0.01\leq x\leq 0.43$ while surface-field acceleration is dominant for $Ga_xIn_{1-x}As$ with $0.43\leq x\leq 0.64$. The magnitude of terahertz emission due to optical rectification is a function of the polycrystal grain size of the $Ga_xIn_{1-x}As$ samples. Terahertz emission from $Ga_xIn_{1-x}As$ due to optical rectification is due to a $\chi^{(2)}$ nonlinear optical process. Overall, terahertz emission from $Ga_xIn_{1-x}As$ is maximized for $x\approx 0.1-0.3$.

DOI: 10.1103/PhysRevB.78.035201 PACS number(s): 78.47.J−, 71.28.+d, 78.20.Jq, 95.85.Gn

I. INTRODUCTION

Binary III-V compound semiconductor materials have received great attention as potential sources of terahertz frequency electromagnetic radiation. GaAs,[1–7] GaSb,[2,4,8,9] InN,[10–12] InP,[2,4,13,14] InAs,[4–6,11,15–30] and InSb[15,17,31–33] have demonstrated emission of subpicosecond terahertz-radiation pulses upon irradiation with femtosecond near-infrared laser pulses. This type of terahertz radiation source has enabled the development of time-domain terahertz spectroscopy and terahertz imaging over the last decade.[34] However, important applications of these techniques in basic and applied science such as nonlinear terahertz spectroscopy, nondestructive testing, or biomedical imaging are still limited by the power of the available sources.[35] The development of bright, high bandwidth terahertz-radiation sources is important in order to expand the applications of these techniques.[36]

Terahertz-radiation emission from binary III-V compound semiconductors exposed to femtosecond near-infrared laser pulses originates either from a nonlinear optical process or ultrafast photocurrents. Nonlinear optical processes in semiconductors resulting in terahertz-radiation emission are bulk[3,13] or surface-field induced optical rectification[23,27] of the incident femtosecond near-infrared laser pulses. Terahertz-radiation emission due to ultrafast photocurrents can be achieved through acceleration of photocarriers by intrinsic or extrinsic electric fields. Intrinsic electric fields occurring at a semiconductor surface are surface depletion/accumulation fields[2] or a Photo-Dember field.[37] Extrinsic electric fields are generated by applying a voltage laterally across a gap between two metal electrodes deposited on the semiconductor surface (photoconducting switch).[38]

InAs, a narrow band-gap semiconductor ($Eg=0.36$ eV) has demonstrated the strongest terahertz-radiation emission of all III-V semiconductor systems characterized to date.[20] The origin of terahertz-radiation emission from InAs is primarily attributed to the Photo-Dember effect[15,20,21,28,30] and surface-field induced optical rectification.[23,24,26,27] Conversely, GaAs, a semiconductor with a wider band gap ($Eg=1.42$ eV) has shown terahertz-radiation emission dominated by different physical phenomena. In GaAs, dominant terahertz-radiation mechanisms are acceleration of carriers by a surface depletion field[2,6,30] and bulk optical rectification.[3]

The III-V ternary alloy semiconductor $Ga_xIn_{1-x}As$ is a very interesting terahertz materials system. It is expected to exhibit properties physically related to both binary systems InAs and GaAs. Moreover, the band gap of $Ga_xIn_{1-x}As$ can be tuned from 0.36 to 1.42 eV by variation of the Ga mole fraction from $x=0$ to $x=1$.[39] Therefore, $Ga_xIn_{1-x}As$ is an attractive material system for compact and lightweight time-domain terahertz spectroscopy and imaging systems powered by femtosecond fiber lasers with emission wavelengths between 0.75 and 1.55 μm.

However, ternary compound semiconductors such as $Ga_xIn_{1-x}As$ are extremely difficult to grow as bulk crystals and are not commercially available.[40] Hence, very limited research has been carried out on terahertz emission from this material.[41–44] Only a few compositions of $Ga_xIn_{1-x}As$ thin films were researched previously. All previous research was limited to $Ga_xIn_{1-x}As$ thin films grown by molecular-beam epitaxy on binary substrates. Furthermore, research was restricted to study terahertz emission from $Ga_xIn_{1-x}As$ photoconductive switches.

In this article, we present an experimental study of femtosecond near-infrared excited terahertz emission of $Ga_xIn_{1-x}As$. In contrast to previous work, we investigate bulk $Ga_xIn_{1-x}As$ crystals grown by the vertical Bridgman method over a wide alloy composition range $0\leq 0.64\leq x$. Furthermore, we focus on the investigation of terahertz-radiation emission by the bare $Ga_xIn_{1-x}As$ surface. We investigate in-depth the relationship between electrical and structural properties of bulk $Ga_xIn_{1-x}As$ and terahertz-radiation emission. We demonstrate that primarily optical rectification and surface-field acceleration contribute to terahertz emission from $Ga_xIn_{1-x}As$ depending on the Ga mole fraction x. We show that emission of terahertz radiation from $Ga_xIn_{1-x}As$ is maximized for x in the range of 0.1–0.3.

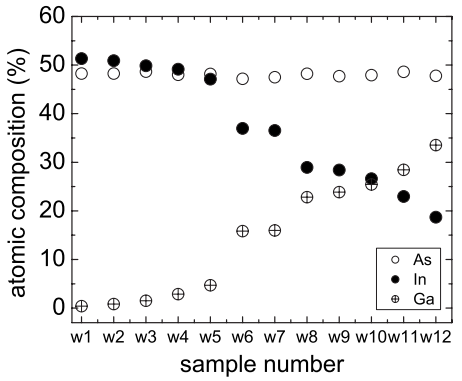

FIG. 1. Measured atomic composition of $Ga_xIn_{1-x}As$ samples.

II. EXPERIMENTAL ARRANGEMENTS

$Ga_xIn_{1-x}As$ ingots were grown by the vertical Bridgman technique and the gradient freezing methods, namely vertical and horizontal gradient freeze techniques.[40,45] After crystal-growth $Ga_xIn_{1-x}As$, ingots were sliced into wafers of 1 mm thickness by a Low Speed Diamond Wheel Saw 660 from South Bay Technology. An Omnilap 2000 wafer polishing unit from South Bay Technology was used for lapping and polishing of the wafers. The lapped wafers were first polished with 1 μm alumina slurry on a nylon pad. Mirrorlike shining surfaces were achieved by a second polishing with 0.01 μm alumina slurry on a velvet pad.

Electrical characterization of our $Ga_xIn_{1-x}As$ samples was performed using a HEM–2000 EGK Hall Measurement System from EGK Co. Hall measurements were performed at 77and 300 K with 0.37 or 0.51 T of magnetic flux and 1 mA of input current. The percentage errors for the measured electrical parameters were 3% for mobility, 2% for resistivity, and 2% for carrier concentrations.

An JEOL-733 electron probe microanalyzer (EPMA) was used to characterize the atomic composition of the $Ga_xIn_{1-x}As$ crystals. Samples were coated with approximately 200 Å of carbon using a Denton Vacuum DV–502A high-vacuum carbon evaporator. Calibration data was obtained using Probe Laboratory standards of GaAs and InAs for Ga, In and As. Data analysis was performed using GELLER ANALYTICAL DQUANT32 software. The Henrich model was used for the ZAF correction. The band gap of our $Ga_xIn_{1-x}As$ crystals were measured by Fourier-transform infrared spectroscopy (FTIR).

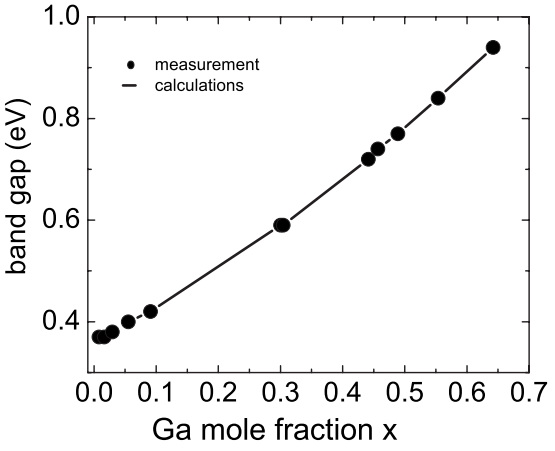

FIG. 2. $Ga_xIn_{1-x}As$ band gap as function of Ga mole fraction at room temperature. Measurements of the band gap were performed by FTIR. Calculations of the band gap of $Ga_xIn_{1-x}As$ were performed according to the equation listed in Table I.

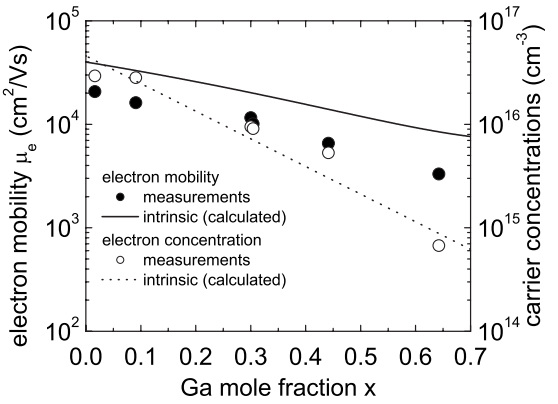

FIG. 3. Measured electron mobility and electron concentrations of the $Ga_xIn_{1-x}As$ samples. Calculations of the electron concentrations and electron mobility of intrinsic $Ga_xIn_{1-x}As$ have been performed according to the equations listed in Table I. The measured electron concentrations and electron mobilities of our samples exhibit the same functional dependence on Ga mole fraction x as the intrinsic electron concentrations and intrinsic mobilities.

Electron beam backscattering diffraction (EBSD) was used to determine the crystallinity of our $Ga_xIn_{1-x}As$ samples and the crystallographic orientations of the surface of the grains. EBSD measurements were performed by an environmental scanning electron microscope FEI/Phillips XL30 ESEM-FEG, a Nordlys I EBSD detector by HKL Technology Inc. and with an HKL CHANNEL 5 software package.

The time-domain terahertz-emission measurement setup that was used for this work is an optical pump-probe arrangement.[46] A commercial diode-pumped titanium-sapphire laser delivers pulses with a duration of 130 fs at a wavelength of 800 nm. The repetition rate is 82 MHz and the maximum average power is 700 mW. The laser beam is split into a pump beam and a probe beam using an uncoated glass as a beam splitter. The power ratio is typically 95% on the pump beam and 5% on the probe beam. Emission from unbiased semiconductor surfaces is achieved by exposing the surface to the pump light beam. The pump beam is slightly focused at the semiconductor surface with a laser spot size of 1 mm^2 and an injected carrier density of approximately 10^{17} cm^{-3}. Measurements were performed setting the angle between the laser beam and the surface's normal to 45°. The pulsed terahertz radiation is detected through electro-optic sampling[47] using a ⟨110⟩ ZnTe crystal of 1 mm thickness. The bandwidth of our electro-optic terahertz detector is limited to 3 THz.

III. RESULTS AND DISCUSSIONS

The alloy compositions of our $Ga_xIn_{1-x}As$ samples as obtained by electron probe microanalysis (EPMA) are illus-

TABLE I. Electrical properties of $Ga_xIn_{1-x}As$ [Ref. 39]

Band gap E_g (eV)	$0.36+0.63x+0.43x^2$
Intrinsic carrier concentration $n_i(cm^{-3})$	$4.38\times10^{15}[(0.41+0.09x)^{3/2}+(0.027+0.047x)^{3/2}]^{1/2}$ $\times(0.025+0.043x)^{3/4}\times[T^{3/2}e^{-v/2}(1+3.75/v$ $+3.28/v-2.46/v)^{1/2}]$ with $v=E_g(x,T)/kT$
Electron mobility $\mu_n(cm^2/Vs)$	$(40-80.7x+49.2x^2)10^3$
Hole mobility $\mu_p(cm^2/Vs)$	300–400
Effective electron mass m_n	$(0.023+0.037x+0.003x^2)m_0$
Effective heavy-hole mass m_{ph}	$(0.41+0.1x)m_0$
Effective light hole mass m_{pl}	$(0.026+0.056x)m_0$
m_0	9.11×10^{-31} kg

trated in Fig. 1. In our samples, the Ga mole fraction varies between $x=0.01$ to $x=.64$. The band gap of the $Ga_xIn_{1-x}As$ samples was determined by FTIR absorption measurements and range from $E_g=0.36$ eV to $E_g=0.94$ eV (Fig. 2). The measured values of the $Ga_xIn_{1-x}As$ band gap agree very well with the empirical relation between band gap E_g and Ga mole fraction x.

The as-grown undoped $Ga_xIn_{1-x}As$ samples are n type as determined by Hall-effect measurements. Unintentionally doped GaAs and InAs are n type in nature due to native defects such as group V element vacancies and group V in group III element antisites. Electron carrier concentrations and electron mobilities of all $Ga_xIn_{1-x}As$ samples are displayed as a function of Ga mole fraction x in Fig. 3. The electron concentrations and electron mobilities decrease exponentially with Ga mole fraction x. This is expected because the band gap of $Ga_xIn_{1-x}As$ widens as the Ga mole fraction x increases. The experimentally obtained electron mobilities are about a factor of two lower than expected for intrinsic $Ga_xIn_{1-x}As$. The lower mobilities observed in our samples are attributed to carrier concentrations higher than in intrinsic material. This reduces the mobilities because of carrier-carrier scattering.

Among all $Ga_xIn_{1-x}As$ samples, samples W1, W5–W8, and W12 were selected for EBSD analysis and terahertz measurements. Table II provides a summary of the alloy composition, conductivity type, carrier concentrations, mobilities, and band gaps for these samples at 300 K.

An orientation contrast image of $Ga_{0.01}In_{0.99}As$ (W1) is displayed in Fig. 4. The image reveals that the sample has large area domains with good crystalline quality. The area of the domains varies with Ga mole fraction x. The largest domains are observed in $Ga_{0.01}In_{0.99}As$ and the smallest domains are found in $Ga_{0.64}In_{0.36}As$. The average domain size varies between (0.196 ± 0.042) and (0.795 ± 0.240) mm^2. The average domain size shrinks with increasing Ga mole fraction x.

Full crystallographic orientation data of the domains are obtained by EBSD. The orientation of a domain is expressed by three Euler angles ϕ, θ, ψ which describe the relationship between sample reference coordinate (x', y', and z') and crystallographic coordinate (a, b, and c). The measured Euler angles demonstrate that the overall disorientations among the domains are small.

We observed emission of terahertz-frequency electromagnetic radiation from all investigated $Ga_xIn_{1-x}As$ samples with $0.01\leq x\leq0.64$. The terahertz transients and frequency spectra emitted by $Ga_{0.01}In_{0.99}As$ and $Ga_{0.64}In_{0.36}As$ are displayed as examples in Fig. 5. We observe that $Ga_{0.01}In_{0.99}As$ exhibits stronger terahertz emission than $Ga_{0.64}In_{0.36}As$. Normalized terahertz frequency spectra for $Ga_{0.01}In_{0.99}As$ and $Ga_{0.64}In_{0.36}As$ are illustrated in Fig. 6. We observe that $Ga_{0.01}In_{0.99}As$ emits terahertz radiation with a slightly broader bandwidth than $Ga_{0.64}In_{0.36}As$.

Furthermore, we have investigated the terahertz emission from $Ga_xIn_{1-x}As$ as a function of the angle between the linear polarization of the excitation laser beam and the crystallographic orientation of the $Ga_xIn_{1-x}As$ surface for the entire compositional range $(0.01\leq x\leq0.64)$. For this experiment, the $Ga_xIn_{1-x}As$ sample was rotated with the surface normal as axis of rotation. The terahertz emission from $Ga_xIn_{1-x}As$ was measured in reflection as a function of azimuth angle ϕ. The results of those measurements for $Ga_{0.01}In_{0.99}As$ and $Ga_{0.64}In_{0.36}As$ are illustrated as examples in Fig. 7. We ob-

TABLE II. Electrical and structural properties of $Ga_xIn_{1-x}As$ samples at 300 K

Sample	Ga (x)	In ($1-x$)	Band gap	Carrier concentration cm^{-3}	doping	Hall mobility (cm^2/Vs)	Domain size (mm^2)
W1	0.01	0.99	0.37	3.25×10^{16}	n type	20700	0.795 ± 0.240
W5	0.09	0.91	0.42	2.83×10^{16}	n type	16174	0.542 ± 0.160
W6	0.29	0.71	0.59	9.49×10^{15}	n type	11601	0.458 ± 0.087
W7	0.30	0.70	0.59	9.08×10^{15}	n type	10100	0.398 ± 0.079
W8	0.44	0.56	0.72	5.30×10^{15}	n type	6566	0.335 ± 0.077
W12	0.64	0.36	0.94	6.74×10^{14}	n type	3320	0.196 ± 0.043

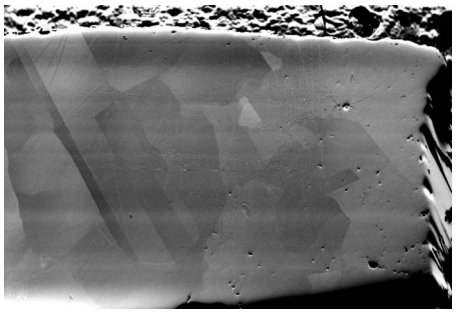

FIG. 4. Orientation contrast image of W1. The sample exhibits large area domains with good crystalline quality.

served that the magnitude of terahertz emission is a function of the angle ϕ between the polarization of the laser beam and $Ga_xIn_{1-x}As$ surface orientation. The magnitude of terahertz emission changes periodically as a function of angle ϕ. The amplitude of the oscillations is larger for $Ga_{0.01}In_{0.99}As$ than $Ga_{0.64}In_{0.36}As$. For $Ga_{0.01}In_{0.99}As$ the oscillation minima are close to zero. For $Ga_{0.64}In_{0.36}As$, the oscillation minima are significantly larger than zero. Our measurements of the whole compositional range reveal that the oscillation amplitude shrinks with increasing Ga mole fraction x whereas the oscillation minima rise with increasing Ga mole fraction (Fig. 8). Within the errors of our measurement, terahertz emission from $Ga_xIn_{1-x}As$ is maximized for $x \approx 0.1-0.3$.

We attribute the origin of the oscillating part of the observed terahertz signal to optical rectification of the incident femtosecond near-infrared laser pulses at the $Ga_xIn_{1-x}As$ surface. Terahertz emission at the oscillation minima is explained by transient photocurrents. Our results demonstrate that terahertz generation in $Ga_xIn_{1-x}As$ is almost entirely due to optical rectification for very small Ga mole fraction $x = 0.01$. Terahertz generation due to optical rectification decreases in $Ga_xIn_{1-x}As$ with increasing mole fraction x. Terahertz generation due to ultrafast currents in $Ga_xIn_{1-x}As$ increases with increasing mole fraction x.

Next, we discuss why terahertz generation in $Ga_xIn_{1-x}As$ due to optical rectification decreases with increasing Ga mole fraction. The amplitude of a terahertz radiation pulse generated by optical rectification in a nonlinear optical crystal depends on the following parameters: (i) amount of optical laser radiation transmitted into the crystal, (ii) crystallographic orientation of the crystal, (iii) the nonlinear electric susceptibility of the crystal, and (iv) microcrystal grain size.

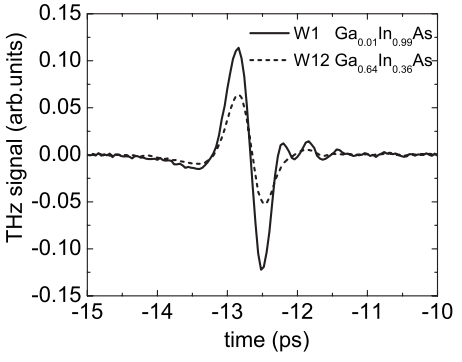

FIG. 5. Time-domain measurements of terahertz radiation pulses emitted by $Ga_xIn_{1-x}As$.

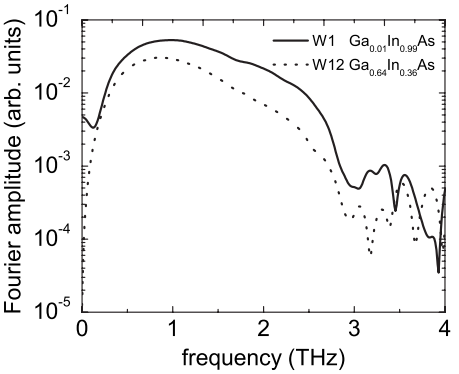

FIG. 6. Frequency spectra of radiation pulses emitted by $Ga_xIn_{1-x}As$.

We have examined all these parameters for $Ga_xIn_{1-x}As$. The amount of laser radiation transmitted into the crystal depends on the index of refraction. The indices of refraction of both InAs and GaAs at 800 nm differ only by ~1% (Table III). Consequently, the amount of laser radiation transmitted into the $Ga_xIn_{1-x}As$ crystals basically does not change as function of Ga mole fraction x. Therefore, it is ruled out that terahertz generation in $Ga_xIn_{1-x}As$ due to optical rectification decreases with increasing Ga mole fraction because the amount of laser radiation transmitted into the material decreases.

Our EBSD data demonstrate that the domains in the $Ga_xIn_{1-x}As$ crystals exhibit very similar crystallographic orientations versus the direction of incidence and polarization of the near-infrared laser beam. Therefore, the variations in terahertz generation from our $Ga_xIn_{1-x}As$ crystals as function of Ga mole fraction x cannot be explained by a change of the crystallographic orientation of the crystal.

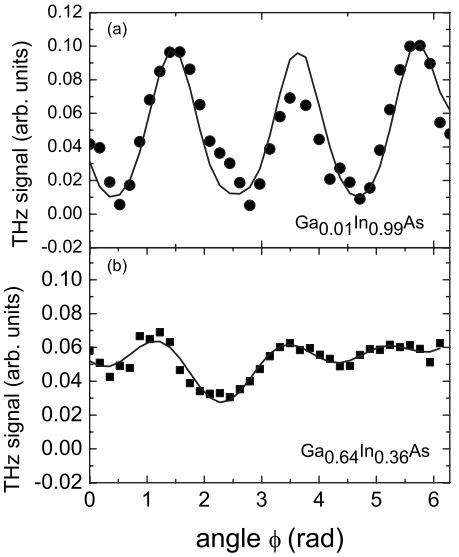

FIG. 7. For this experiment, the $Ga_xIn_{1-x}As$ sample was rotated with the surface normal as axis of rotation. The terahertz emission from $Ga_xIn_{1-x}As$ was measured in reflection as a function of azimuth angle ϕ. The terahertz signal oscillates as a function of the angle Φ.

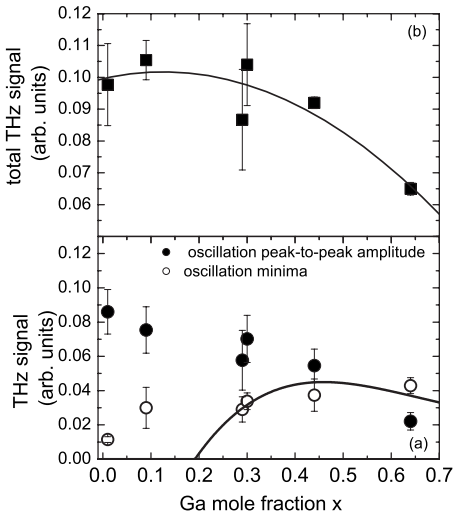

FIG. 8. (a) Total terahertz emission from $Ga_xIn_{1-x}As$ as function of Ga mole fraction x. The data are averages of the oscillation maxima measured between 0 rad $\leq\Phi\leq$6.3 rad. The solid line is a guide to the eye. (b) Peak-to-peak amplitude of the oscillating part of the terahertz signal and oscillation minima of the terahertz signal. Again, the data displayed are the averages measured between 0 rad $\leq\Phi\leq$6.3 rad. The solid line describes the calculated terahertz emission due to surface-field acceleration.

Terahertz radiation generated by optical rectification in InAs and GaAs has been investigated experimentally previously. Terahertz generation in InAs was attributed to surface-field induced optical rectification whereas terahertz generation in GaAs was explained by bulk optical rectification. The magnitude of terahertz generation due to surface-field induced optical rectification is determined by the third order nonlinear electric susceptibility of the material and terahertz generation due to bulk optical rectification depends on the second-order nonlinear electric susceptibility. The explanation of strong terahertz emission from InAs by surface-field optical rectification was previously supported by the argument that the third order susceptibility of a narrow band-gap semiconductor such as InAs is several orders of magnitude larger than the third order susceptibility of a wider band-gap material such as GaAs. However, a closer examination of the calculated third order susceptibilities of InAs and GaAs[49,50] reveal that the third order susceptibility of InAs $\chi^{(3)}\approx10^{-7}$ esu is only larger than the third order susceptibility of GaAs $\chi^{(3)}\approx10^{-10}$ esu for the case of resonant excitation (laser photon energy $\approx$ band gap) of both materials. In our experiments, $Ga_xIn_{1-x}As$ crystals are excited at 800 nm wavelength (E_{photon}=1.55 eV). For GaAs, the laser photon energy is resonant with the band gap of the material whereas for InAs the laser photon energy is significantly larger than the band gap. The values of $\chi^{(2)}$ and $\chi^{(3)}$ of InAs and GaAs at 800 nm wavelength are summarized in Table III. The summary demonstrates that the third order nonlinear susceptibility of InAs at 800 nm is approximately zero. The second-order nonlinear susceptibilities $\chi^{(2)}$ of InAs and GaAs are around 1×10^{-6} esu, the third order nonlinear susceptibility of GaAs is $1.\times10^{-10}$ esu. Based on the magnitudes of $\chi^{(2)}$ and $\chi^{(3)}$ for GaAs and InAs at 800 nm, we explain terahertz generation due to optical rectification in $Ga_xIn_{1-x}As$ to be dominated by the $\chi^{(2)}$ nonlinear optical process. Since $\chi^{(2)}$ of InAs and GaAs have approximately the same magnitude $\chi^{(2)}\approx10^{-6}$ esu, we expect that the amplitude of terahertz radiation emitted by In-rich $Ga_xIn_{1-x}As$ samples is the same order of magnitude than terahertz radiation emitted by Ga-rich $Ga_xIn_{1-x}As$ samples. This expectation is in agreement with our experimental observations.

Next, we discuss the influence of crystal size on terahertz generation by optical rectification. The efficacy of a nonlinear optical process depends on the coherence length.[51] If the refractive indices of the near-infrared laser excitation frequency and the terahertz radiation are identical, then the strength of terahertz emission would increase similarly for all frequencies within the bandwidth with increasing crystal thickness. However, the refractive indices for the near-infrared laser frequency and terahertz frequency are generally not identical in $Ga_xIn_{1-x}As$ (Table III). Consequently, electromagnetic waves at terahertz- and near-infrared frequencies travel at slightly different speeds through the crystal. The efficacy of nonlinear optical terahertz generation decreases if the mismatch between the velocities becomes too large. The distance over which the slight velocity mismatch can be tolerated is the coherence length. As a result, the efficacy of terahertz generation due to optical rectification will decrease if the crystal thickness is less than the coherence length. We have measured the domain size A of our $Ga_xIn_{1-x}As$ crystals (Table II). We define $l=A^{1/2}$ as a characteristic length of the domain. We observe that l decreases with increasing Ga mole fraction $0.01\leq x\leq0.64$. We have plotted the terahertz signal, due to optical rectification, as a function of characteristic domain size l (Fig. 9) and observe a positive linear correlation between terahertz signal due to optical rectification and characteristic domain size l. We have performed a linear regression analysis of the data displayed in Fig. 9 and found a coefficient of correlation r=0.96. The decrease of terahertz emission due to optical rectification is explained by a reduced efficacy of the nonlinear optical process. The efficacy of optical rectification decreases in Ga-rich $Ga_xIn_{1-x}As$ because of a smaller polycrystal grain size.

TABLE III. Optical properties of InAs and GaAs

Optical properties	InAs	GaAs
Index of refrection at 800 nm n_{opt} [48]	3.729	3.679
Index of refrection at 1 THz n_{THz} [48]	3.778	3.60
Second order susceptibility $\lvert\chi^{(2)}\rvert$ at 800 nm (esu)[49]	1.3×10^{-6}	1.5×10^{-6}
Third order susceptibility $\lvert\chi^{(3)}\rvert$ at 800 nm (esu)[50]	≈0	$\approx1.\times10^{-10}$

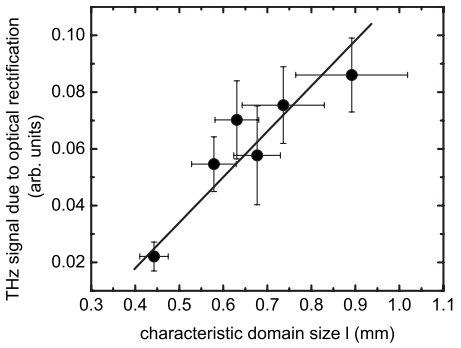

FIG. 9. Positive linear correlation between terahertz signal due to optical rectification and characteristic domain size *l*. The solid line represents a linear regression analysis. The coefficient of correlation is $r=0.96$.

Terahertz generation proceeds by optical rectification or by the transport of photoexcited free carriers.[20] The current surge induced by photoexcitation has two sources: (1) the acceleration of photoexcited carriers by the surface depletion field caused by Fermi-level pinning, and (2) the photo-Dember effect originating from the difference between the diffusion constants of electrons and holes.[15] The origin of the surface-field effect is band bending due to Fermi-level pinning by surface states.[21] A charge distribution at the surface forms a built-in electric field directed normal to the surface. When an ultrafast laser pulse illuminates a semiconductor surface with photon energy greater than the band gap of the material, electron-hole pairs are created at the semiconductor surface. The photogenerated carriers are accelerated by the built-in electric field to form a transient photocurrent which in turn generates terahertz radiation. The other mechanism known as photo-Dember effect originates from the charge-carrier density gradient caused by the photogenerated carriers near the surface which drives diffusion of electrons and holes into the material. A charge-carrier density gradient is formed due to the higher mobility of electrons compared to the mobility of holes. This diffusion current in turn generates terahertz radiation. In a narrow band-gap III–V compound semiconductors such as InAs the origin of current-surge induced terahertz emission is the photo-Dember effect whereas in wide band-gap semiconductor such as GaAs the surface-field acceleration effect is the responsible physical mechanism.[21]

We have calculated for $Ga_xIn_{1-x}As$ the radiated terahertz-electric field E_{far} due to surface-field acceleration and the photo-Dember effect as a function of Ga mole fraction x. The calculations are performed according to Eq. (1) (photo-Dember effect) and Eq. (2) (surface-field acceleration).

$$E_{far} = \frac{S}{4\pi\varepsilon_o c^2 \tau r} \frac{k_B T_e \mu_n}{(1+b)} \left[\frac{b(n_b - p_b)}{1+b} \ln\left(1 + \frac{G(1+b)}{p_b + bn_b}\right) - G \right] \tag{1}$$

$$E_{far} = \frac{Se^2 \mu_n G |N_D^+ - N_A^-|}{4\pi\varepsilon_0^2 \varepsilon_r c^2 \tau r c \alpha^2} [W\alpha - 1 + e^{-\alpha W}] \tag{2}$$

As derived previously,[23] the magnitude of terahertz radiation emitted due to the photo-Dember effect [Eq. (1)] depends on the electron and hole concentrations n_b and p_b, the ratio of electron and hole mobilities $b=\mu_n/\mu_h$ and the electron temperature T_e.

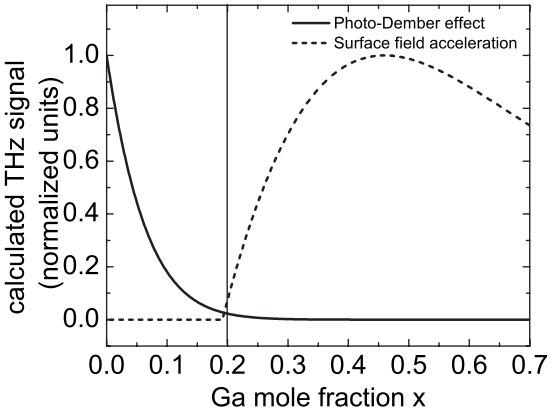

FIG. 10. Calculations of the terahertz signal due to the photo-Dember effect and surface-field acceleration in $Ga_xIn_{1-x}As$ as a function of Ga mole fraction x. Calculated terahertz signals are normalized to 1. The absolute magnitude of the two mechanisms is not considered.

The magnitude of terahertz radiation emitted due to surface-field acceleration [Eq. (2)] depends on depletion width $W=(2\varepsilon_r\varepsilon_0\Phi_s/\rho)^{1/2}$, surface potential Φ_s, charge in the depletion region $\rho=q(p-n+N_D^+-N_A^-)\approx q(N_D^+-N_A^-)$, N_D^+, N_A^- donor and acceptor concentrations and absorption depth α. Furthermore, in Eqs. (1) and (2), S is the laser focal spot size, τ is the laser-pulse duration, r is the distance in the far field, and G is the photocarrier generation rate. Also, in Eqs. (1) and (2) $\varepsilon_0=8.85\times10^{-12}$ As/Vm, $c=3.00\times10^8$ m/s and ε_r is the permittivity of the semiconductor.

The terahertz-emission from $Ga_xIn_{1-x}As$ as a function of Ga mole fraction x is calculated using the intrinsic parameters[39] $\mu_n(x)$, $\mu_p(x)$, $n_b(x)$, $p_b(x)$, $k_bT_e(x)=1.55$ eV $-E_g(x)=(1.19+0.63x+0.43x^2)$ eV and $G(x)=(2.45+30(1-x))\times10^8$ cm^{-3} in Eq. (1). We justify using intrinsic parameters by the observation that our measured electron carrier concentrations and electron mobilities exhibit the same functional dependence on Ga mole fraction x as the intrinsic properties. (Fig. 3)

The terahertz emission due to the photo-Dember mechanism and surface-field acceleration for $Ga_xIn_{1-x}As$ is illustrated in Fig. 10 as a function of the Ga mole fraction x. Our calculations demonstrate that terahertz emission is expected to be dominated by the photo-Dember effect for $x\leq0.2$ whereas terahertz emission due to surface-field acceleration is inexistent in this compositional range. Terahertz emission due to the Photo-Dember effect becomes neglible for $x\geq0.2$. Terahertz emission due to surface-field acceleration increases for $x\geq0.2$ and reaches a maximum at $x\approx0.45$.

The photo-Dember effect dominates terahertz-emission for $0<x<0.2$ because the surface depletion field is negligible for these alloy compositions in $Ga_xIn_{1-x}As$. Surface Fermi-level pinning in III–V compound semiconductors is caused by surface states associated with defects present at the surface of the semiconductor.[52] The dominant types of surface state for most semiconductors are acceptors located within the band gap [71]. However, surface defect states in

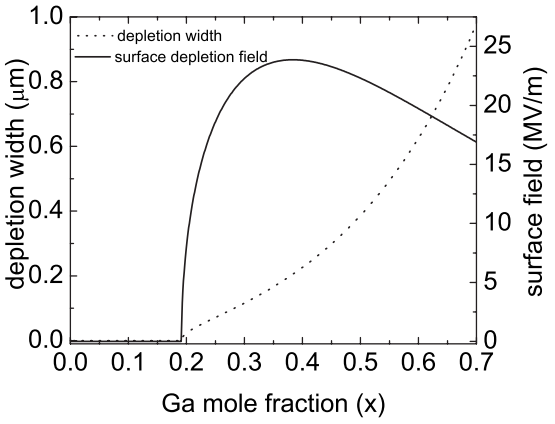

FIG. 11. Depletion width W and surface depletion field E_s in $Ga_xIn_{1-x}As$ as a function of Ga mole fraction.

InAs are donors and are located above the minimum of the conduction-band edge.[53] This leads to an electron accumulation layer at the surface of InAs. The sheet electron concentration of the accumulation layer is typically about 1×10^{12} cm^{-2} and is unaffected by bulk doping of InAs.[53] Fermi-level pinning in InAs occurs for any InAs surface orientation. The energy difference between the conduction-band minimum and the Fermi-level energy in $Ga_xIn_{1-x}As$ can be expressed as $E_F^*=(0.43x^2+0.502x-0.102)$ eV. According to this equation, the Fermi-level reaches the minimum of the conduction band in $Ga_xIn_{1-x}As$ for $x \approx 0.2$. The corresponding surface field $E_s=\rho(W-z)/(\varepsilon_r\varepsilon_0)$ and depletion width W are calculated for $Ga_xIn_{1-x}As$ as a function of Ga mole fraction x and illustrated in Fig. 11. Again, our calculations demonstrate that surface depletion field is negligible for $0<x<0.2$. The surface field exhibits a maximum at $x \approx 0.35$. The depletion width W monotonically increases with Ga mole fraction x for $x>0.2$. The terahertz emission due to surface-field acceleration depends on the integral over the photocurrent $E_{far} \propto \int_0^w j(z)dz$ with $j(z) \propto G(z)E_s(z)$. This relationship results in a maximum of terahertz emission at $x \approx 0.45$. We explain that terahertz emission from $Ga_xIn_{1-x}As$ is due to ultrafast currents being dominated by surface-field acceleration for $x>0.2$.

We do not observe a strong contribution to terahertz emission from ultrafast currents in $Ga_{0.01}In_{99}As$. For this composition, terahertz emission appears to be entirely due to optical rectification. This is a surprising observation considering the results of previous measurements of terahertz emission from InAs. In experiments performed on ⟨100⟩ oriented InAs crystals, the terahertz emission was found to be due to the photo-Dember effect. This is in agreement with predictions by nonlinear optics which rule out optical rectification for this orientation. In previous experiments on ⟨110⟩ and ⟨111⟩ oriented InAs crystals the observation was made that terahertz emission is due to optical rectification as well as ultrafast currents. However, the terahertz generation due to optical rectification was generally weaker than terahertz generation due to ultrafast currents. In addition, optical rectification was generally observed for excitation by amplified titanium-sapphire laser pulses which provide much stronger optical electric fields than our titanium-sapphire oscillator. Our observation suggests that the mechanism and magnitude of terahertz emission from InAs depends on the microstructure of the InAs crystal. The microstructure of InAs crystals is influenced by the crystal-growth process. We suggest that further research on terahertz emission from InAs should focus on the effect of crystal growth and microstructure of the material on terahertz emission.

IV. CONCLUSIONS

We have studied femtosecond optically excited emission of terahertz radiation from bulk $Ga_xIn_{1-x}As$ crystals over a large compositional range. We identified optical rectification of the incident femtosecond near-infrared laser pulses and acceleration of photocarriers by a surface depletion field as terahertz emission mechanisms in our $Ga_xIn_{1-x}As$ crystals. Terahertz emission from In-rich $Ga_xIn_{1-x}As$ is dominated by optical rectification of the femtosecond laser pulses. Terahertz emission from Ga-rich $Ga_xIn_{1-x}As$ is primarily due to surface-field acceleration of photocarriers. The magnitude of the terahertz emission due to optical rectification increases with polycrystal grain size in our $Ga_xIn_{1-x}As$ samples. According to our measurements and analysis, terahertz emission from In-rich as well as Ga-rich $Ga_xIn_{1-x}As$ is due to a $\chi^{(2)}$ nonlinear optical process. We found that terahertz emission from $Ga_{0.01}In_{0.99}As$ is caused entirely by optical rectification. Terahertz emission due to surface-field acceleration is maximized in $Ga_xIn_{1-x}As$ with $x \approx 0.45$. This is explained by a maximum of the surface depletion field for this composition of $Ga_xIn_{1-x}As$. The overall terahertz emission from bulk $Ga_xIn_{1-x}As$ crystals is the strongest in the $x \approx 0.1-0.3$ compositional range.

ACKNOWLEDGMENTS

We would like to thank E. B. Watson and J. Thomas for suggesting EBSD for structural analysis of our samples. Furthermore, we acknowledge technical support of EBSD measurements by Zhenting Jiang at Yale University. This material is based upon work supported by the National Science Foundation under Grant No. 0333314.

[1] X.-C. Zhang, B. Hu, J. Darrow, and D. Auston, Appl. Phys. Lett. **56**, 1011 (1990).
[2] X.-C. Zhang and D. H. Auston, J. Appl. Phys. **71**, 326 (1992).
[3] X. C. Zhang, Y. Jin, K. Yang, and L. J. Schowalter, Phys. Rev. Lett. **69**, 2303 (1992).
[4] C. Weiss, R. Wallenstein, and R. Beigang, Appl. Phys. Lett. **77**, 4160 (2000).
[5] J. N. Heyman, P. Neocleous, D. Hebert, P. A. Crowell, T. Muller,

and K. Unterrainer, Phys. Rev. B **64**, 085202 (2001).
[6] J. Heyman, N. Coates, A. Reinhardt, and G. Strasser, Appl. Phys. Lett. **83**, 5476 (2003).
[7] M. Nagai, K. Tanaka, H. Ohtake, T. Bessho, T. Sugiura, T. Hirosumi, and M. Yoshida, Appl. Phys. Lett. **85**, 3974 (2004).
[8] S. Winnerl, S. Sinning, T. Dekorsy, and M. Helm, Appl. Phys. Lett. **85**, 3092 (2004).
[9] R. Ascazubi, C. Shneider, I. Wilke, R. Pino, and P. S. Dutta, Phys. Rev. B **72**, 045328 (2005).
[10] R. Ascazubi, I. Wilke, K. Denniston, H. Lu, and W. J. Schaff, Appl. Phys. Lett. **84**, 4810 (2004).
[11] G. Chern, E. Readinger, H. Shen, M. Wraback, C. Gallinat, G. Koblmueller, and J. Speck, Appl. Phys. Lett. **89**, 141115 (2006).
[12] B. Pradarutti, G. Matthaeus, C. Brueckner, S. Riehemann, G. Notni, S. Nolte, V. Cimalla, V. Lebedev, O. Ambacher, and A. Tuennermann, Proc. SPIE **6194**, 619401 (2006).
[13] P. N. Saeta, B. I. Greene, and S. L. Chuang, Appl. Phys. Lett. **63**, 3482 (1993).
[14] M. Nakajima, M. Hangyo, M. Ohta, and H. Miyazaki, Phys. Rev. B **67**, 195308 (2003).
[15] S. Kono, P. Gu, M. Tani, and K. Sakai, Appl. Phys. B: Lasers Opt. **B71**, 901 (2000).
[16] R. McLaughlin, Q. Chen, A. Corchia, C. M. Ciesla, D. D. Arnone, X.-C. Zhang, G. A. C. Jones, E. H. Linfield, and M. Pepper, J. Mod. Opt. **47**, 1847 (2000).
[17] P. Gu, M. Tani, S. Kono, K. Sakai, and X.-C. Zhang, J. Appl. Phys. **91**, 5533 (2002).
[18] M. B. Johnston, D. M. Whittaker, A. Corchia, A. G. Davies, and E. H. Linfield, Phys. Rev. B **65**, 165301 (2002).
[19] M. P. Hasselbeck, D. Stalnaker, L. A. Schlie, T. J. Rotter, A. Stintz, and M. Sheik-Bahae, Phys. Rev. B **65**, 233203 (2002).
[20] H. Takahashi, A. Quema, R. Yoshioka, S. Ono, and N. Sarakura, Appl. Phys. Lett. **83**, 1068 (2003).
[21] H. Takahashi, A. Quema, R. Yoshioka, S. Ono, and N. Sarakura, Jpn. J. Appl. Phys., Part 2 **42**, L1259 (2003).
[22] R. Yano, H. Gotoh, Y. Hirayama, S. Miyashita, Y. Kadoya, K. Kusuda, and M. Yamanishi, J. Appl. Phys. **95**, 2141 (2004).
[23] R. Adomavicius, A. Urbanowicz, G. Molis, A. Krotkus, and E.·Satkovskis, Appl. Phys. Lett. **85**, 2463 (2004).
[24] R. Adomavičius, G. Molis, A. Krotkus, and V. Sirutkaitis, Appl. Phys. Lett. **87**, 1 (2005).
[25] R. Mendis, M. L. Smith, L. J. Bignell, R. E. M. Vickers, and R. A. Lewis, J. Appl. Phys. **98**, 126104 (2005).
[26] M. Reid and R. Fedosejevs, Proc. SPIE **5577**, 659 (2004).
[27] M. Reid, I. V. Cravetchi, and R. Fedosejevs, Phys. Rev. B **72**, 035201 (2005).
[28] K. Liu, J. Xu, T. Yuan, and X. C. Zhang, Phys. Rev. B **73**, 155330 (2006).
[29] E. Estacio, H. Sumikura, H. Murakami, M. Tani, N. Sarukura, M. Hangyo, C. Ponseca, R. Pobre, R. Quiroga, and S. Ono, Appl. Phys. Lett. **90**, 151915 (2007).
[30] D.-F. Liu and D. Xu, Appl. Opt. **46**, 789 (2007).
[31] S. Howells, S. Herrera, and L. Schlie, Appl. Phys. Lett. **65**, 2946 (1994).
[32] H. Takahashi, Y. Suzuki, M. Sakai, S. Ono, N. Sarukura, T. Sugiura, T. Hirosumi, and M. Yoshida, Appl. Phys. Lett. **82**, 2005 (2003).
[33] R. Ascazubi, I. Wilke, K. J. Kim, and P. Dutta, Phys. Rev. B **74**, 075323 (2006).
[34] *Sensing with Terahertz Radiation*, edited by D. Mittleman (Springer-Verlag, New York, 2003).
[35] *Terahertz Spectroscopy: Principles and Applications*, edited by S. L. Dexheimer (CRC, Boca Raton, FL/Taylor & Francis, London, 2008).
[36] B. Ferguson and X.-C. Zhang, Nat. Mater. **1**, 26 (2002).
[37] T. Dekorsy, H. Auer, H. J. Bakker, H. G. Roskos, and H. Kurz, Phys. Rev. B **53**, 4005 (1996).
[38] C. Fattinger and D. Grischkowsky, Appl. Phys. Lett. **53**, 1480 (1988).
[39] M. Levinshtein, S. Rumayantsev, and M. S. Shur, *Handbook Series on Semiconductor Parameters* (World Scientific, Singapore, 1996).
[40] P. Dutta, J. Cryst. Growth **275**, 106 (2005).
[41] C. Baker, I. S. Gregory, W. R. Tribe, I. V. Bradley, M. J. Evans, M. Withers, P. F. Taday, V. P. Wallace, E. H. Linfield, A. G. Davies, and M. Missous, Appl. Phys. Lett. **83**, 4113 (2003).
[42] M. Suzuki and M. Tonouchi, Appl. Phys. Lett. **86**, 051104 (2005).
[43] N. Chimot, J. Mangeney, P. Crozat, J. M. Lourtioz, K. Blary, J. F. Lampin, G. Mouret, D. Bigourd, and E. Fertein, Opt. Express **14**, 1856 (2006).
[44] A. Takazato, M. Kamamura, T. Matsui, J. Kitagawa, and Y. Kadoya, Appl. Phys. Lett. **90**, 101119 (2007).
[45] P. S. Dutta, in *Crystal Growth Technology*, edited by H. J. Scheel and P. Capper (Wiley, Weinheim, 2008), Chap. 12.
[46] J. Shah, *Ultrafast Spectroscopy of Semiconductors and Semiconductor Heterostructures* (Springer, New York, 1996).
[47] Q. Wu, M. Litz, and X.-C. Zhang, Appl. Phys. Lett. **68**, 2924 (1996).
[48] E. Palik, *Handbook of Optical Constants of Solids* (Academic, San Diego, 1998).
[49] M.-Z. Huang and W. Y. Ching, Phys. Rev. B **47**, 9464 (1993).
[50] W. Y. Ching and M. Z. Huang, Phys. Rev. B **47**, 9479 (1993).
[51] A. Nahata, A. S. Weling, and T. F. Heinz, Appl. Phys. Lett. **69**, 2321 (1996).
[52] H. Wieder, Appl. Phys. Lett. **38**, 170 (1981).
[53] C. Affentauschegg and H. Wieder, Semicond. Sci. Technol. **16**, 708 (2001).